Test of gamma-ray strength functions in nuclear reaction model calculations

J. Kopecky
Netherlands Energy Research Foundation ECN, P.O. Box 1, 1755 ZG Petten, The Netherlands

M. Uhl
Institut für Radiumforschung und Kernphysik, Universität Wien, A1090 Wien, Boltzmanngasse 3, Austria
(Received 25 October 1989)

The impact of models for $E1$ and $M1$ gamma-ray strength functions on the results of nuclear model calculations of total average radiation widths, radiative capture cross sections, and gamma-ray spectra has been studied. We considered strength functions that reproduce photoabsorption and/or average resonance data but significantly differ from each other at low gamma-ray energies. As the calculated quantities critically depend on the strength functions in this energy region, model calculations can be used to test the low-energy behavior of strength functions. By analyzing the ^{197}Au, ^{143}Nd, ^{105}Pd, and ^{93}Nd neutron capture reactions we found strong evidence for a model of the $E1$ strength function, which is characterized by the following properties: (i) an energy dependent spreading width of the underlying Lorentzian for the photoabsorption cross section and (ii) a nonzero, temperature dependent, limit as the transition energy tends to zero. This model is founded in theoretical work by Zaretskij, Sirotkin, and Kadmenskij and represents a partial breakdown of Brink's hypothesis.

I. INTRODUCTION

Gamma-ray strength functions characterize the average electromagnetic properties of excited nuclei. Beside their fundamental importance for nuclear structure, gamma-ray strength functions are an indispensable tool for applied nuclear reaction model calculations. The transmission coefficients $T_{XL}(\varepsilon_\gamma)$ of multipole type XL, which enter into the gamma-ray emission rates, are proportional to the corresponding strength functions $f_{XL}(\varepsilon_\gamma)$.

The simplest model for the strength functions, the single-particle model,[1] results in energy independent strength functions. However, a large amount of information shows that in case of the predominant $E1$ radiation the single-particle model overestimates the experimental data by far.[2,3]

Reaction theory relates the (downwards) strength function for a given multipole type to the corresponding absorption cross section. The calculation of photoabsorption cross sections for excited states is carried out in exactly the same way as for the ground state by assuming the giant resonance built on each excited state. With this hypothesis Brink[4] calculated gamma-ray emission rates in terms of experimental (extrapolated) photoabsorption cross sections. Combined with the giant dipole resonance (GDR) model for the absorption of the predominant $E1$ radiation this celebrated "Brink hypothesis" was the keystone for most analyses of gamma-ray strength functions (see, e.g., Refs. 5, 6, and 2) and of many calculations of capture cross sections and of gamma-ray production spectra (see, e.g., Refs. 7–10). Evidence has grown that the strength functions for $M1$ and $E2$ radiation may also be related to a corresponding giant resonance (see, e.g., Refs. 11–14).

Simple semiclassical models predict a Lorentzian shape for the photon absorption cross section dominated by a giant resonance. Accurate measurements of the primary $E1$ radiation from neutron resonances indicate that the GDR model describes the experimental data much better than the single-particle model. Nevertheless, the simple Lorentzian shape of the absorption cross section proves inadequate at energies close to the neutron binding energy. Various empirical prescriptions have been proposed to correct for insufficiencies of the shape of the $E1$ absorption cross section such as, e.g., a "depressed" Lorentzian[15] or an "energy dependent Breit-Wigner" shape.[16] A comprehensive compilation of functional forms for the GDR can be found in Gardner's review.[17] The uncertainties in the parametrization of the $E1$ absorption cross section affect the ability to calculate capture cross sections and gamma-ray spectra. As a consequence, such calculations often use relative strength functions of a given shape and apply some normalization. A popular approach is to normalize the $M1$, $E2, \ldots,$ strength relative to the predominant $E1$ contribution and to find the absolute value of the latter by reproducing the ratio $\langle \Gamma_{\gamma 0} \rangle / \langle D_0 \rangle$ of the average radiation width and the average spacing of s-wave neutron resonances.

More detailed models for the $E1$ strength function have been proposed by Zaretskij and Sirotkin,[18] Kadmenskij *et al.*,[19] and Sirotkin.[20] These rely on the theory of Fermi liquids and account for microscopic properties of the GDR. Essential predictions are an energy dependent spreading width of the resonance and a nonzero limit of the strength function $f_{E1}(\varepsilon_\gamma)$ as the transition energy ε_γ tends to zero. As the spreading width and the $\varepsilon_\gamma \rightarrow 0$ limit depend on the temperature of the final state, these more

realistic models are at variance with the Brink hypothesis. Kopecky and Chrien[14] recently analyzed the $E1$ strength function deduced from average resonance capture (ARC) data for ^{105}Pd+n in terms of a generalized Lorentzian exhibiting the two essential features of these theories. A simultaneous reproduction of the photoabsorption cross section and the $E1$ strength function was achieved. Unfortunately the energy range covered by the ARC data was not large enough to validate the $\varepsilon_\gamma \to 0$ limit. Support for these strength function models stems from the analysis of quite distinct experimental data: the alpha spectra from $(n,\gamma\alpha)$ reactions at thermal energies[21] and the yrast feeding pattern resulting from (heavy-ion, $xn\gamma$) reactions.[22]

In this paper we study the impact of models for $E1$ and $M1$ strengths on nuclear reaction model calculations. For $E1$ radiation we consider a standard Lorentzian and two generalizations of it, in particular, one that allows for a nonzero $\varepsilon_\gamma \to 0$ limit of $f_{E1}(\varepsilon_\gamma)$ (Ref. 14) and for $M1$ radiation, on the other hand, either a giant resonance of Lorentzian shape or the single-particle model. For four spherical target nuclei we calculate for incident neutrons the average total s-wave radiation width, (average) capture cross sections, and gamma-ray spectra and compare them to available experimental data. The strength functions employed for $E1$ and $M1$ radiation are chosen so as to reproduce independent experimental information such as photoabsorption cross sections and/or resonance capture data. No further normalizations are adopted. Besides the improvement of nuclear reaction model calculations our main aim is the verification of the nonzero $\varepsilon_\gamma \to 0$ limit of the $E1$ strength function.

The next section presents a detailed specification of the strength functions employed in this paper. A description of the model calculations and of the underlying parameters follows. Subsequently the results are compared with experimental data. The last section summarizes the conclusions.

II. GAMMA-RAY STRENGTH FUNCTIONS

A. Adopted formalism for $E1$, $M1$, and $E2$ strength functions

1. $E1$ radiation

As has been mentioned in the Introduction, the large amount of information on primary $E1$ radiation indicates that the Brink formulation overestimates the experimental gamma-ray strength functions at and below the neutron binding energy B_n. In order to study this effect in model calculations we have used the three following different definitions of the gamma-ray strength functions.

(a) The standard Lorentzian expression. Here the Lorentzian line shape with energy independent damping width has been employed, as used for the photoabsorption cross sections. This expression corresponds to the original approach of Brink[4] and reads as

$$f_{E1}(\varepsilon_\gamma)=8.68\times10^{-8}(\text{mb}^{-1}\,\text{MeV}^{-2})\frac{\sigma_0\varepsilon_\gamma\Gamma^2}{(\varepsilon_\gamma^2-E^2)^2+\varepsilon_\gamma^2\Gamma^2}\ , \tag{2.1}$$

where σ_0 (mb), Γ (MeV), and E (MeV) are the usual giant resonance parameters derived from photoabsorption experiments and ε_γ is the gamma-ray energy (in MeV).

(b) The Lorentzian with energy dependent damping width. In this case an energy dependence of the damping width has been included, as suggested by Dover *et al.*[23] The following formula for $f_{E1}(\varepsilon_\gamma)$ has a similar form to Eq. (2.1):

$$f_{E1}(\varepsilon_\gamma)=8.68\times10^{-8}(\text{mb}^{-1}\,\text{MeV}^{-2})\times\frac{\sigma_0\varepsilon_\gamma\Gamma\Gamma(\varepsilon_\gamma)}{(\varepsilon_\gamma^2-E^2)^2+\varepsilon_\gamma^2\Gamma(\varepsilon_\gamma)^2}\ , \tag{2.2}$$

where $\Gamma(\varepsilon_\gamma)$ stands for the energy depending damping width. This dependence can be parametrized as a power of ε_γ. The spreading of the giant dipole particle-hole excitations into two-particle, two-hole states suggests that $\Gamma(\varepsilon_\gamma)$ is proportional to ε_γ^2. Further, Kadmenskij *et al.*[19] pointed out that, in addition to the ε_γ^2 width dependence, a contribution dependent on the temperature of the state on which the giant resonance is built (due to quasiparticle collisions) has to be included. This phenomenon has recently been verified experimentally in proton or heavy-ion capture experiments (see, e.g., Ref. 24). We adopted the formulation from Ref. 19, which is based on the Fermi liquid theory, and can be written as

$$\Gamma(\varepsilon_\gamma)=\Gamma\frac{\varepsilon_\gamma^2+4\pi^2T^2}{E^2}\ , \tag{2.3}$$

where $T=\sqrt{(B_n-\varepsilon_\gamma)/a}$ is the nuclear temperature; the symbol a is the Fermi gas level density parameter and B_n represents the neutron binding energy. For simplicity we omitted a pairing correction in the temperature definition since its influence on the present calculations is small.

(c) The generalized Lorentzian. This expression takes into account the difficulty, first pointed out in Ref. 23, that the extrapolation of the Lorentzian function to $\varepsilon_\gamma \to 0$ is unjustified. In several papers Kadmenskij *et al.*,[19] Zaretskij,[18] and Sirotkin[20] emphasized this point and proposed various treatments to account for the failure of the Lorentzian function to describe the electric dipole operator in the limit of zero energy. We have accepted the limiting value of $f_{E1}(\varepsilon_\gamma)$ for $\varepsilon_\gamma \to 0$ as derived in Ref. 19. However, we have used the alternative formula, proposed by Chrien[25] and used in Refs. 14 and 26, namely to add $f_{E1}(0,T)$ as given by Kadmenskij *et al.*[19] to correct the Lorentzian expression given in Eq. (2.2). This results in the expression

$$f_{E1}(\varepsilon_\gamma,T)=8.68\times10^{-8}(\text{mb}^{-1}\,\text{MeV}^{-2})\times\left[\frac{\varepsilon_\gamma\Gamma(\varepsilon_\gamma)}{(\varepsilon_\gamma^2-E^2)^2+\varepsilon_\gamma^2\Gamma(\varepsilon_\gamma)^2}+\frac{0.7\Gamma 4\pi^2T^2}{E^5}\right]\sigma_0\Gamma\ . \tag{2.4}$$

This form is correct in the low-energy limit and differs from the Lorentzian negligibly at the neutron binding energy B_n and therefore it is reasonable to expect Eq. (2.4) to be valid over the whole region of neutron capture gamma rays. It is not valid near the $E1$ giant resonance peak.

(d) The pigmy resonance. For the ^{93}Nb and ^{197}Au targets a pigmy resonance was adopted in accordance with experimental information and recent systematics.[8,26,31] The shape was assumed to have a Lorentzian form, as given in Eq. (2.1), and the resonance parameters have been derived from the fit to the experimental data in Figs. 1 and 4. The contribution of the pigmy resonance has been incoherently added to the corresponding f_{E1} functions as given by Eqs. (2.2) and (2.4). For the standard Lorentzian expression no pigmy resonance was assumed because the predicted strength function is well above the experimental data and the inclusion of this resonance shall make the fit even worse.

2. *M1 radiation*

Two prescriptions have been used for the distribution of the $M1$ strength in the present study. In the (adjusted) single-particle model[1] the fragmented strength is adjusted to the experimental data for the primary $M1$ transitions, correcting a global overestimation by this model. The second choice is a giant resonance model based on the existence of the $M1$ giant resonance assumed to be related to shell-model spin-flip transitions between $l\pm\frac{1}{2}$ single-particle states (see Bohr and Mottelson[27]). The interpretation of primary $M1$ radiation within this model was investigated in Refs. 13, 14, and 26 and a reasonable agreement was found both for the shape of the proposed strength function and for the energy-weighted $M1$ strength.

The collective $M1$ giant resonance is described by a Lorentzian with energy independent damping width and we ignore the temperature dependence as well. Both these simplifications are justified because the region of interest is not the tail of the giant resonance but rather the resonance itself; under these assumptions $f_{M1}(\varepsilon_\gamma)$ is also given by Eq. (2.1). There is still a very limited amount of information on the $M1$ giant resonance parameters. Thus, it is very difficult to establish any systematics. We adopted the following values, as in Ref. 27, namely $E=41A^{-1/3}$ (MeV), $\Gamma=4$ (MeV), and the value of σ_0 adjusted either to experimental data or else derived from the f_{E1}/f_{M1} systematics[28] at energies close to the neutron binding energy.

3. *E2 radiation*

The strength of many observed pure $E2$ primary transitions is again well reproduced by the giant resonance model.[12] However, for lower masses ($A<130$) the single-particle model fits the primary data equally well. We adopted the first model, which seems to be valid more generally and gives the consistency of using essentially the same model for all three multipolarities. Thus, the $E2$ strength function $f_{E2}(\varepsilon_\gamma)$ is described by a similar equation to Eq. (2.1):

$$f_{E2}(\varepsilon_\gamma)=5.22\times10^{-8}(\text{mb}^{-1}\,\text{MeV}^{-2})\times\frac{\sigma_0\varepsilon_\gamma^{-1}\Gamma^2}{(\varepsilon_\gamma^2-E^2)^2+\varepsilon_\gamma^2\Gamma^2}\ . \tag{2.5}$$

The parametrization of the $E2$ giant resonance parameters is based on well-documented systematics: $E=63A^{-1/3}$ (MeV) (Ref. 29), $\Gamma=(6.11-0.012A)$ (MeV) (Ref. 12), and $\sigma_0=1.5\times10^{-4}Z^2E^2A^{-1/3}/\Gamma$ (mb) (Ref. 12). The contribution of $E2$ radiation to the calculated cross sections is very small and the inclusion of a generalized Lorentzian seemed to us, at this point of the investigation, unnecessary.

B. Comparison with experimental data

The parameters employed for the derivation of the strength functions, as defined in Eqs. (2.1) to (2.5), are

TABLE I. The strength function parameters employed in the calculations.

		^{198}Au	^{144}Nd	^{106}Pd	^{94}Nb
$E1$	σ_0 (mb)	541	317	199	200
	E (MeV)	13.72	15.05	15.92	16.59
	Γ (MeV)	4.61	5.28	7.18	5.05
	σ_p (mb)[a]	6.00			1.50
	E_p (MeV)[a]	5.80			6.80
	Γ_p (MeV)[a]	1.50			1.90
$M1$	σ_0 (mb)	1.12	0.37	1.06	1.39
	E (MeV)	7.05	7.82	8.80	9.02
	Γ (MeV)	4.00	4.00	4.00	4.00
	SP_{adj} (W.U.)[b]	0.48	0.14	0.38	0.26
$E2$	σ_0 (mb)	5.03	3.40	2.46	2.14
	E (MeV)	10.81	12.02	13.31	13.86
	Γ (MeV)	3.73	4.38	4.84	4.98

[a]Pigmy resonance.
[b]Adjusted single-particle model.

given in Table I. In order to check how the constructed strength functions fit the experimental information, the calculated curves are plotted in Figs. 1–4, together with available data either from the average resonance capture experiments[14,30] or from discrete resonance capture data.[2]

No adjustment was applied to the calculated strength functions and only σ_0 for the $M1$ giant resonance or the magnitude of the $M1$ single-particle prediction has been derived from experiment. The absolute magnitude of all f_{E1} data is derived from the discrete resonance capture data based on the absolute normalization to the 4.9-eV Au resonance.

The inspection of calculated gamma-ray strength functions as shown in Figs. 1–4, shows that, in general, *all* primary gamma-ray transitions are well reproduced by the assumed functions, except for the standard Lorentzian which overestimates the $E1$ data. There is no direct way, however, to test the f_{E1} or f_{M1} distribution below a gamma-ray energy of 3 MeV. Such primary transitions are difficult to observe and corresponding data are not available.

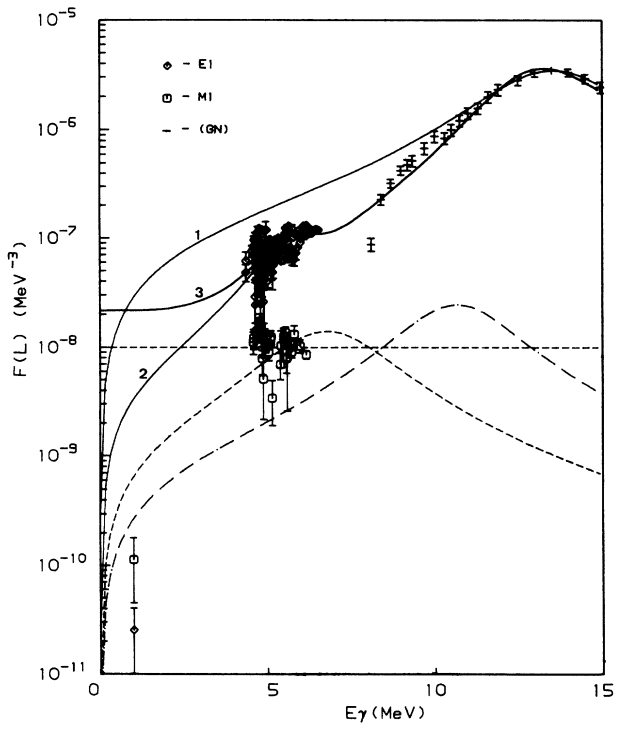

FIG. 1. The measured (Ref. 30) primary photon strength functions for the ^{197}Au(n,γ) reaction plotted versus gamma-ray energy; the photoabsorption data (GN) were taken from Ref. 32. Parameters used for the pigmy resonance are given in Table I. The calculated strength functions, discussed in the text, are plotted as solid, dashed, and dashed-dotted curves for $E1$, $M1$, and $E2$ radiation, respectively. The different $E1$ models are denoted as standard Lorentzian [Eq. (2.1)→1], Lorentzian with energy dependent damping width [Eq. (2.2)→2], and generalized Lorentzian [Eq. (2.4)→3]. The f_{M1} curves are self-explanatory. The curves and data points for the $E2$ radiation are multiplied by ε_γ^2. The points at 1 MeV are values derived from Ref. 33, see text.

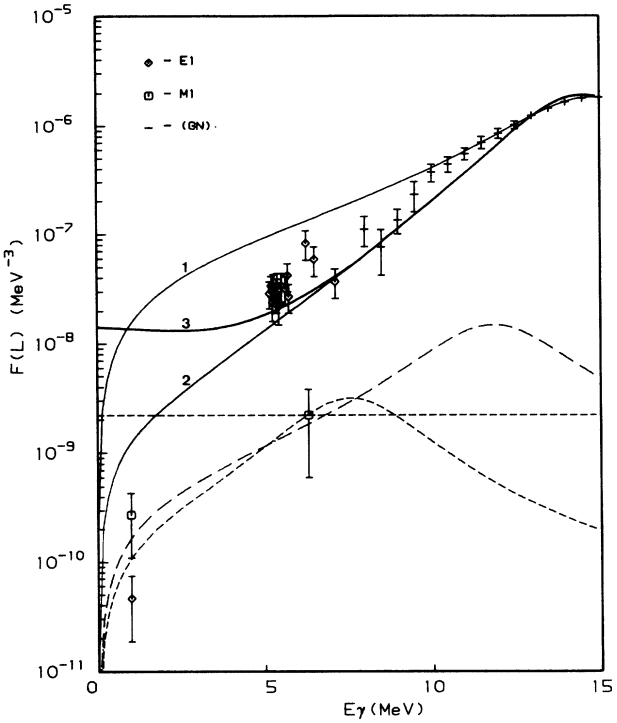

FIG. 2. The same as Fig. 1 for the ^{143}Nd(n,γ) reaction (primary strength function data, Ref. 2).

In the spirit of the Brink hypothesis, if it is fully valid, the reduced strength should be equal to that of the transitions with the same energy at *any* excitation. We have used transitions between bound states of low excitations ($E_x < 2$ MeV) with empirical hindrance factors ($\langle\Gamma_{exp}\rangle/\langle\Gamma_{sp}\rangle$) compiled by Endt[33] for nuclei with

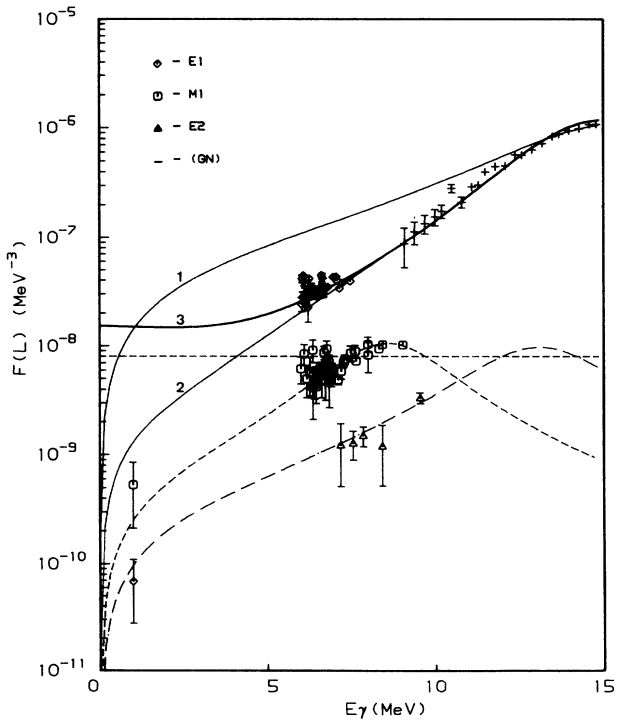

FIG. 3. The same as Fig. 1 for the ^{105}Pd(n,γ) reaction (primary strength function data, Ref. 14).

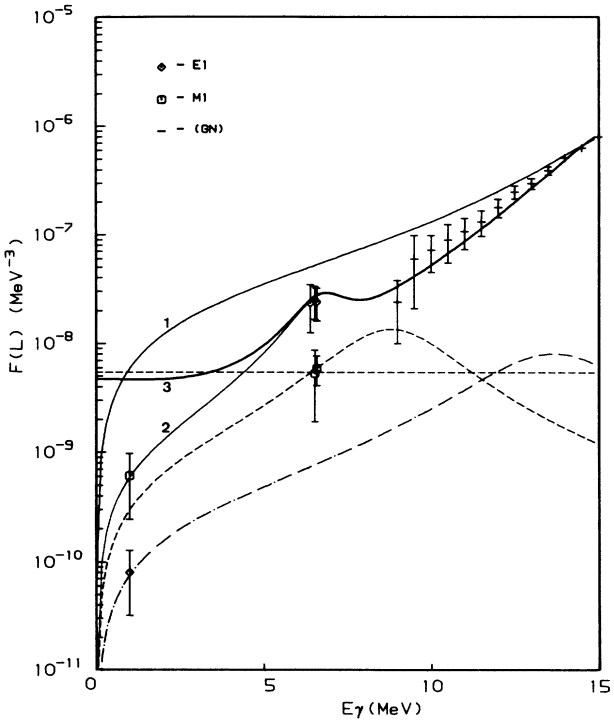

FIG. 4. The same as Fig. 1 for the ^{93}Nb(n,γ) reaction (primary strength function data, Ref. 2). Parameters used for the pigmy resonance are given in Table I.

$A < 150$. The corresponding strength functions for 1 MeV were deduced from the estimated mean values for $E1$ and $M1$ hindrance factors as a function of A.[34] They are plotted in Figs. 1–4 (for ^{198}Au extrapolated hindrance factors were used). The error bars represent the full width at half maximum value of the distributions of the hindrance factors estimated from plots in Ref. 33. The results differ significantly for both f_{E1} and f_{M1} given by the generalized Lorentzian and the adjusted $M1$ single-particle model, respectively. The discrepancy between f_{E1} and the generalized Lorentzian is to be expected as the displayed curves refer to primaries from the capture state and so a transition energy of 1 MeV corresponds to final states with an excitation of several MeV. However, for $M1$ radiation this disagreement forms an important argument for the rejection of the adjusted single-particle model. Furthermore, an energy independent f_{M1} is at variance with a finite energy-weighted sum rule of $M1$ strength.

Recently, Schumacher *et al.*[35] compared the above-mentioned empirical hindrance factors for $E1$ radiation with a standard Lorentzian assuming a pure statistical distribution of the radiative width. The comparison with experimental data demonstrates that the distribution of the $E1$ hindrance factors approximately follows a Porter-Thomas distribution and further that the values below the energy of 4 MeV decrease even faster than prescribed by the Lorentzian. This second conclusion supports the present results displayed in Figs. 1–4.

Based on these arguments it seems that the giant resonance assumption leads to reasonable models both for $M1$ and $E1$ radiation and that the adjusted single-particle model, although fitting $M1$ primary gamma-ray data, fails to explain the experimental information based on the low-energy data from Ref. 33.

III. MODEL CALCULATIONS

The total s-wave radiation widths, the (average) capture cross sections, and the gamma-ray spectra were calculated in the frame of the statistical compound nucleus model. We restrict the incident neutron energies to values below a few MeV where compound nucleus reactions dominate. Other capture mechanisms were neglected so far. The calculations were performed with the code MAURINA.[36] This program applies Moldauer's[37] prescription for the width fluctuation correction; a nonfluctuating lumped channel is assumed for photons. A detailed treatment of gamma-ray cascades as described, e.g., in Ref. 38 allows the calculation of gamma-ray spectra. In connection with this work an option regarding gamma-ray transmission coefficients which depend on the excitation energy of the final state was included. The calculations require the knowledge of several auxiliary quantities or parameters.

The *gamma-ray transmission coefficients* $T_{XL}(\varepsilon_\gamma)$ for multipole type XL are related to the corresponding strength function by

$$T_{XL}(\varepsilon_\gamma)=2\pi\varepsilon_\gamma^{2L+1}f_{XL}(\varepsilon_\gamma)\ .$$

For $E1$, $M1$, and $E2$ radiation we used the strength functions specified in the previous section. The strengths of $M2$, $E3$, and $M3$ radiation were derived from the single-particle model. The contributions of quadrupole and octupole radiation to the calculated quantities are much smaller than those of dipole radiation and therefore the choice of their strength does not critically affect our conclusions.

The *neutron transmission coefficients* were derived from optical potentials taken from the literature; they are specified for the individual cases below. As the target nuclei considered in this paper are spherical we applied the single-channel optical model. Test calculations with different optical potentials indicated no strong dependence of our results on these quantities. For the four target nuclei we used the neutron potentials given by Joly[9] for ^{197}Au, Wilmore and Hodgson[39] for ^{143}Nd, Van der Kamp and Gruppelaar[40] for ^{105}Pd, and Delaroche *et al.*[41] for ^{93}Nb.

The most important auxiliary quantity is the *level density*. This can easily be seen from the expression for the average total radiation width $\langle\Gamma_\gamma(E,I,\Pi)\rangle$ of compound states with excitation energy E, spin I, and parity Π

$$\langle\Gamma_\gamma(E,I,\Pi)\rangle=\frac{1}{2\pi\rho(E,I,\Pi)}\sum_{XL}\sum_{I_f,\Pi_f}\int_0^E d\varepsilon_\gamma T_{XL}(\varepsilon_\gamma)\rho(E-\varepsilon_\gamma,I_f,\Pi_f)\ , \tag{3.1}$$

TABLE II. The level density parameters employed in the calculations.

	^{198}Au	^{197}Au	^{144}Nd	^{106}Pd	^{94}Nb	^{93}Nb
a (MeV^{-1})	17.48	19.74	14.99	13.84	11.61	10.95
Δ_B (MeV)	−1.10	−0.21	0.69	0.71	−1.18	−0.60
$\tilde{a}$ (MeV^{-1})	27.20	28.26	18.60	15.21	13.06	12.92
Δ_P (MeV)	0.00	0.79	1.94	2.59	0.00	0.72
E_x (MeV)	6.51	5.81	6.42	7.53	4.91	5.88
E_0 (MeV)	−1.72	−0.42	0.61	0.34	−1.61	−0.91
T (MeV)	0.605	0.522	0.603	0.676	0.759	0.782
σ^2_{lev}	5.64	6.60	6.13	5.79	9.97	10.92

where $\rho(E,I,\Pi)$ designates the density of levels with excitation energy around E, with spin I and parity II. The summations over spin I_f and parity Π_f are restricted by the usual selection rules. The total average s-wave radiation width is a weighted average of appropriate contributions $\langle \Gamma_\gamma(E,I,\Pi)\rangle$. Integrals of the same structure also enter into the radiative capture cross sections and the gamma-ray spectra are determined by the products $T_{XL}(\varepsilon_\gamma)\rho(E-\varepsilon_\gamma,I,\Pi)$. For low excitation energy we used in Eq. (3.1) and other similar expressions instead of the level density the actually known levels listed in recent issues of the journal "Nuclear Data Sheets."[42]

Two models for the calculation of the level density were employed: the backshifted Fermi gas model[43] (BSFG model) and the model of Kataria *et al.*[44] (KRK model) which accounts for shell effects in terms of the ground-state shell correction to the nuclear binding energy. The parameters of these models were determined from the average s-wave resonance spacing $\langle D_0\rangle$ and the number of low-lying levels. The $\langle D_0\rangle$ values employed for ^{198}Au, ^{144}Nd, ^{106}Pd, and ^{93}Nb are, respectively, 16.2,[45] 45,[46] 10,[46] and 65 eV.[47] The BSFG model is character-

TABLE III. Calculated and experimental total s-wave radiation widths in MeV.

	Level density: KRK model				Level density: BSFG model				
	$\langle\Gamma_{\gamma0}\rangle_{M1}$	$\langle\Gamma_{\gamma0}\rangle_{E1}$	$\langle\Gamma_{\gamma0}\rangle_{E2}$	$\langle\Gamma_{\gamma0}\rangle$	$\langle\Gamma_{\gamma0}\rangle_{M1}$	$\langle\Gamma_{\gamma0}\rangle_{E1}$	$\langle\Gamma_{\gamma0}\rangle_{E2}$	$\langle\Gamma_{\gamma0}\rangle$	$\langle\Gamma_{\gamma0}\rangle_{\text{expt}}$
^{198}Au	10.1[a]	344.9[a]	5.0[a]	360.0	10.1[a]	366.1[a]	5.6[a]	381.8	128±6 (Ref. 45)
		84.0[b,e]		99.1		76.6[b,e]		92.3	
		127.2[c,e]		142.3		132.5[c,e]		148.2	
	36.7[d]	344.9[a]		386.6	43.4[d]	366.1[a]		415.1	
		84.0[b,e]		125.7		76.6[b,e]		125.6	
		127.2[c,e]		168.9		132.5[c,e]		181.5	
^{144}Nd	1.7[a]	149.1[a]	2.5[a]	153.3	2.5[a]	223.1[a]	3.9[a]	229.5	80±9 (Ref. 46)
		15.9[b]		20.1		24.2[b]		30.7	
		44.5[c]		48.6		73.0[c]		79.5	
	9.7[d]	149.1[a]		161.3	14.9[d]	223.1[a]		241.8	
		15.9[b]		28.2		24.2[b]		43.0	
		44.5[c]		56.7		73.0[c]		91.8	
^{106}Pd	6.8[a]	249.9[a]	3.0[a]	259.8	10.8[a]	416.7[a]	5.0[a]	432.5	145±8 (Ref. 46)
		30.1[b]		40.0		53.8[b]		69.6	
		84.7[c]		94.6		156.2[c]		172.0	
	45.2[d]	249.9[a]		298.1	72.4[d]	416.7[a]		494.2	
		30.1[b]		78.3		53.8[b]		131.3	
		84.7[c]		133.0		156.2[c]		233.7	
^{94}Nb	11.8[a]	148.8[a]	3.5[a]	164.1	16.5[a]	220.9[a]	5.0[a]	242.5	145±10 (Ref. 49)
		28.3[b,e]		43.7		42.2[b,e]		63.8	
		53.3[c,e]		68.6		80.5[c,e]		102.1	
	43.3[d]	148.8[a]		195.6	61.6[d]	220.9[a]		287.6	
		28.3[b,e]		75.2		42.2[b,e]		108.9	
		53.3[c,e]		100.1		80.5[c,e]		147.2	

[a]Lorentzian Eq. (2.1) or (2.5).
[b]Lorentzian with energy dependent damping width Eq. (2.2).
[c]Generalized Lorentzian Eq. (2.4).
[d]Adjusted single-particle model.
[e]Pigmy resonance included.

ized by the level density parameter a and the backshift Δ_B while the parameters of the KRK model are the asymptotic level density parameter $\tilde{a}$ and the fundamental frequency ω for which we used the global prescription $\omega=0.185A^{1/3}$ MeV^{-1} in terms of the mass number A. Actually the model of Kataria *et al.*[44] was supplemented by the prescription of Gilbert and Cameron:[48] application of a conventional pairing shift Δ_P and a constant temperature form $\rho(E)=\exp[(E-E_0)/T]$ which smoothly joins the KRK expression at excitation energy $E=E_x$. For the effective moment of inertia Θ_{eff}, which, via the spin cutoff factor σ, determines the spin dependence of the level density, we assumed the rigid body value $\Theta_{\text{eff}}=\Theta_{\text{rig}}=\frac{2}{5}AR^2$, where A is the mass number and the nuclear radius was assumed to be given by $R=1.25A^{1/3}$. In the case of the KRK model, in the constant temperature region, we linearly interpolated the square σ^2 of the spin cutoff factor between the value σ^2_{lev} deduced from the spin distributions of low-lying levels and the value prescribed by the model at $E=E_x$. Variations of Θ_{eff} indicated some sensitivity of our results to this quantity but not to an extent as to affect our conclusions concerning the gamma-ray strength functions. The level density parameters of all relevant nuclei for $\Theta_{\text{eff}}=\Theta_{\text{rig}}$ are listed in Table II. In general, we assumed an equal parity distribution of the continuous level density. Rough assessments of the effect of this assumption were performed by assuming the expression

$$\rho(E,I,\Pi)=\rho(E,I)f_{\Pi}(E)\ ,$$

where $f_+(E)+f_-(E)=1$. Starting at the continuum edge with the value resulting from the known levels the parity fraction $f_{\Pi}(E)$ (exponentially) approaches the limit 0.5 near the neutron binding energy. Test calculations showed that the effects of the parity dependence on the total radiation width and the capture cross sections did not exceed 10 percent and therefore are not very critical for this investigation.

IV. RESULTS AND DISCUSSION

Uncertainties in the above-described parameters affect the accuracy of the calculations. We emphasize at this point that we did not exploit the uncertainties of the model parameters to improve the reproduction of experimental data as one could try to do in an evaluation by means of model calculations. In fact, this section shows that the agreement between our computations and the experimental data is reasonable but not excellent. However, by achieving a simultaneous description of several and partly independent data, we hope that our conclusions on gamma-ray strength functions hold true in spite of the uncertainties of the model parameters.

A. Total average *s*-wave radiation widths

Table III shows the computed total *s*-wave radiation width $\langle\Gamma_{\gamma 0}\rangle$ along with its three most important components $\langle\Gamma_{\gamma 0}\rangle_{M1}$, $\langle\Gamma_{\gamma 0}\rangle_{E1}$, and $\langle\Gamma_{\gamma 0}\rangle_{E2}$ as well as the experimental results. The calculations were performed for each of the two level density models and under the following different assumptions on the strength functions for dipole radiation. A giant resonance of standard Lorentzian shape and the adjusted single-particle model was employed for $M1$ while for $E1$ we considered, in addition to a standard Lorentzian, also one with an energy dependent spreading width, and further, the generalization resulting in a nonzero $\varepsilon_\gamma\to 0$ limit of $f_{E1}(\varepsilon_\gamma)$ [see Sec. II, in particular, Eqs. (2.1)–(2.5)]. In Table III entries in a given column which agree with those of the previous line are not repeated.

For ^{144}Nd, ^{106}Pd, and ^{94}Nb the two level density models result in rather different radiation widths. As both of them reproduce the same number of low-lying levels and of *s*-wave resonances, the reasons for this effect are the different energy dependences of ρ and the slightly different spin cutoff factors. As an illustration Fig. 5 displays the total level density for ^{106}Pd resulting from the two level density models. The main contributions to the integrals Eq. (3.1) stem from excitation energies a few MeV below the neutron separation energy (=9.56 MeV for ^{106}Pd) where the two models differ by a considerable amount. This eventual difference in the calculated level densities is characteristic for uncertainties of such semiempirical models; for similar reasons to those for the total radiation widths, it affects the calculated capture cross sections and the gamma-ray spectra, too (see below).

According to Eq. (3.1) the total radiation width critically depends on the behavior of the gamma-ray strength functions $f_{XL}(\varepsilon_\gamma)$ in the energy range between zero and a

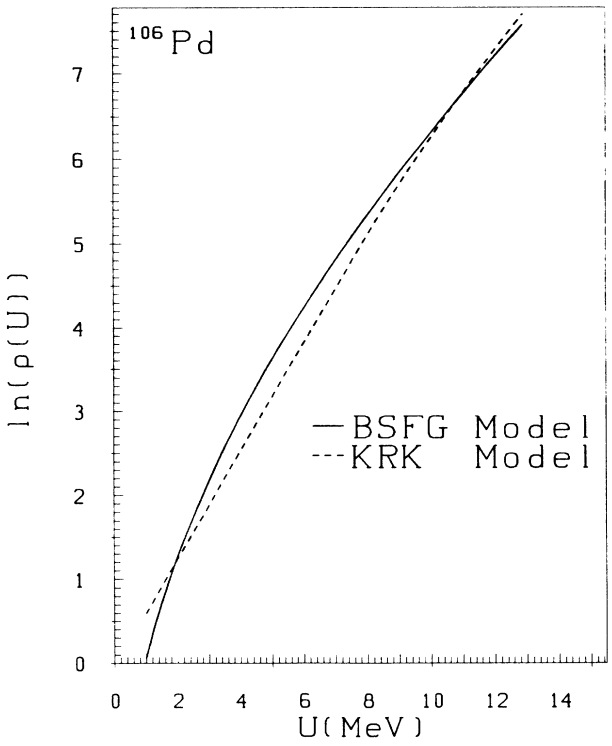

FIG. 5. The total level density of ^{106}Pd obtained with the BSFG and the KRK model (see text) using the parameters listed in Table II. The actual calculations use below $U=2.48$ MeV, the level scheme.

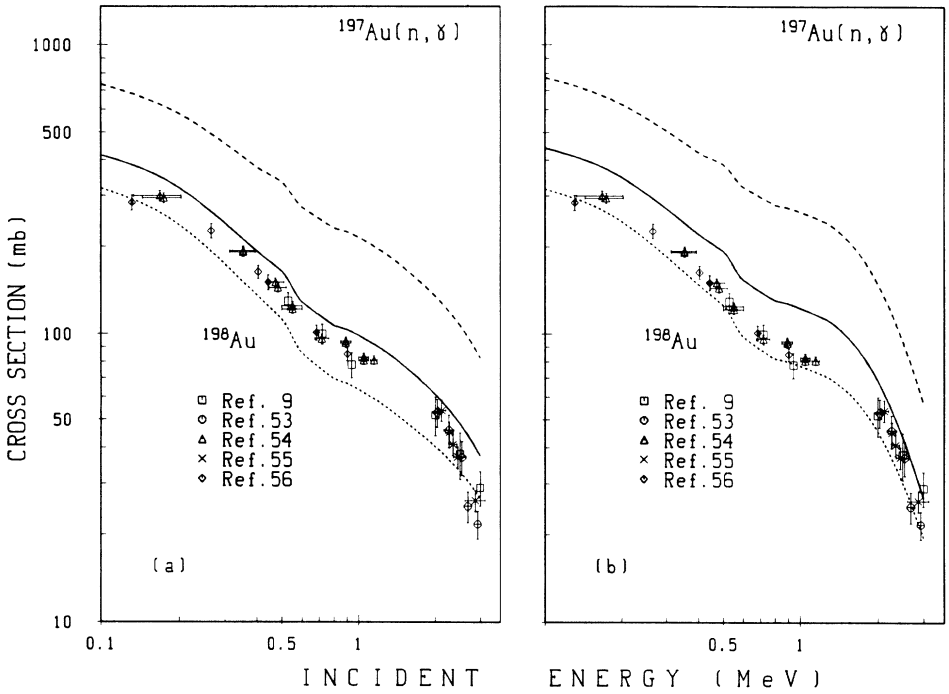

FIG. 6. The ^{197}Au neutron capture cross section calculated with level densities according to (a) the KRK model and (b) the BSFG model. The strength functions of $M1$ and $E2$ radiation were derived from giant resonances of Lorentzian shape. Three different models for the $E1$ strength are used. The dashed curve corresponds to a standard Lorentzian [Eq. (2.1)], the dotted one to a Lorentzian with energy dependent spreading width [Eq. (2.2)], and the full curve to a generalized Lorentzian according to Eq. (2.4). The experimental data were measured by Joly (Ref. 9), Andersson *et al.* (Ref. 53), Dalvetshin *et al.* (Ref. 54), Husain and Hunt (Ref. 55), and Chen Jing *et al.* (Ref. 56).

few MeV where the integrand has a maximum and where no data are available. The large differences between the $E1$ contributions $\langle \Gamma_{\gamma 0} \rangle_{E1}$ obtained with strength functions differing only in the low-energy portion can be noted in Table III. The comparison to experimental data shows that, in general, in accord with the ARC data, the $E1$ strength function based on a standard Lorentzian [Eq. (2.1)] that reproduces the photoabsorption cross-

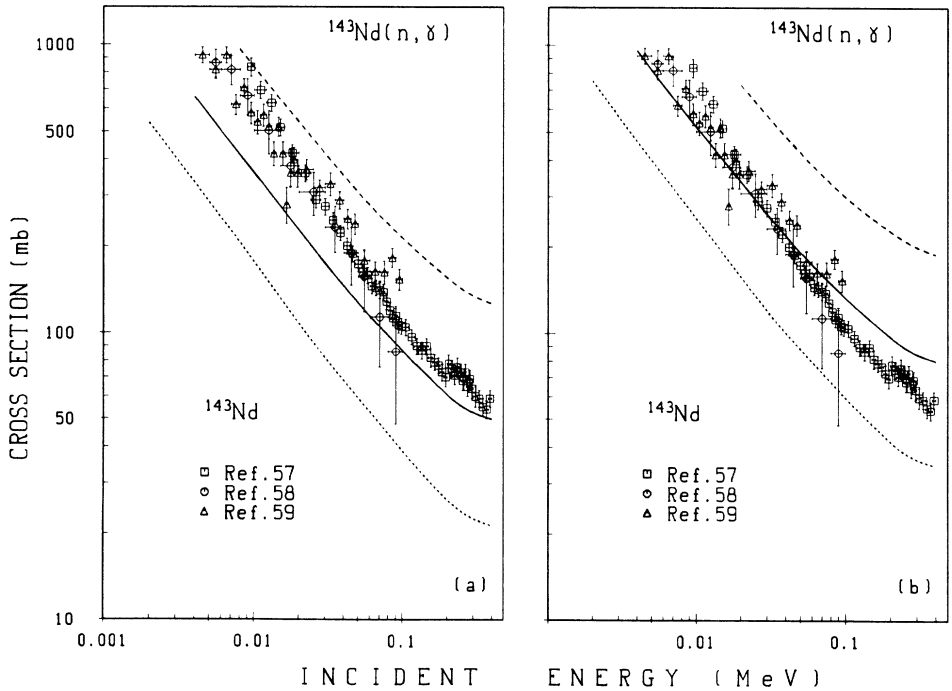

FIG. 7. The same as Fig. 6, but for the neutron capture cross section of ^{143}Nd. The experimental data were measured by Bokovko *et al.* (Ref. 57), Musgrove *et al.* (Ref. 58), and Nakajima *et al.* (Ref. 59).

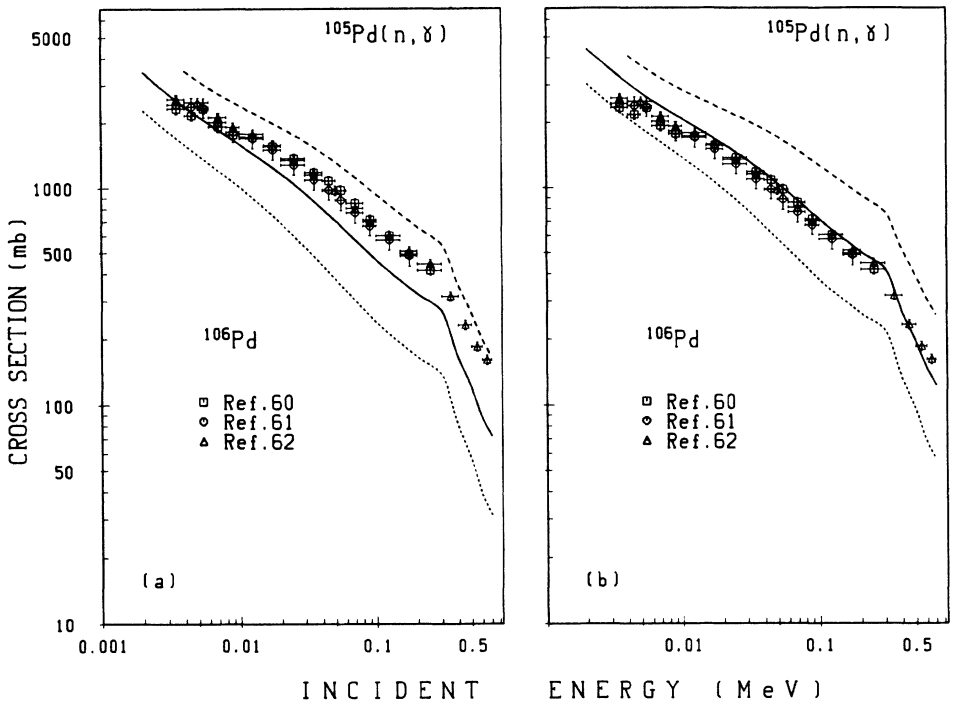

FIG. 8. The same as Fig. 6, but for the neutron capture cross section of ^{105}Pd. The experimental data were measured by Cornelis *et al.* (Ref. 60), Musgrove *et al.* (Ref. 61), and Macklin *et al.* (Ref. 62).

section results in overprediction of total radiation widths, no matter what model is adopted for $M1$ strength. On the other hand, assuming a giant resonance for $M1$ radiation, the $E1$ strength calculated with a Lorentzian with an energy dependent spreading width [Eq. (2.2)] leads to $\langle \Gamma_{\gamma 0} \rangle$ values which are too small, though, in that case, primary gamma-ray transitions are reasonably accounted for. In the case of ^{198}Au, ^{144}Nd, and ^{106}Pd, a reasonable simultaneous reproduction of the total radiation width, the primary gamma-ray data, and the photoabsorption

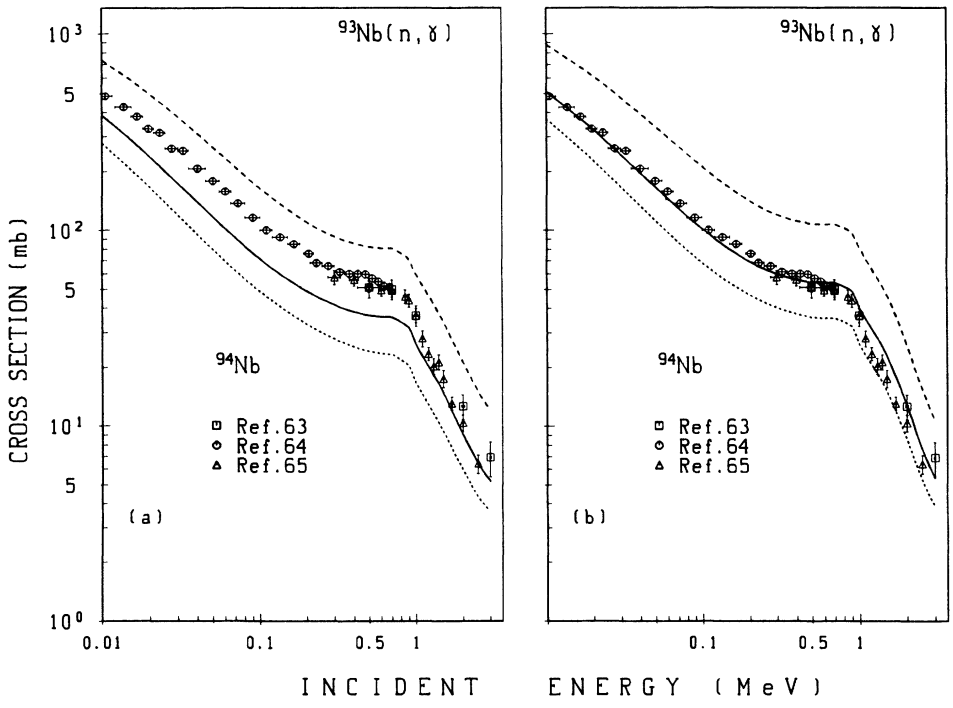

FIG. 9. The same as Fig. 6, but for the neutron capture cross section of ^{93}Nb. The experimental data were measured by Voignier *et al.* (Ref. 63), Macklin (Ref. 64), and Poenitz (Ref. 65).

data is achieved with a standard Lorentzian for $M1$ and a generalized Lorentzian with a nonzero $\varepsilon_\gamma \to 0$ limit [Eq. (2.4)] for $E1$ radiation; in Table III the results corresponding to these models are underlined. In addition, a Lorentzian with an energy dependent spreading width [Eq. (2.2)] for $E1$ combined with the single-particle model for $M1$ adjusted to experimental data cannot be excluded by comparison with the experimental total radiation widths and primary gamma-ray data. However, as discussed in Sec. II an energy independent $M1$ strength is not supported by the experimental information on transitions between low-lying excited levels.

For ^{94}Nb the preferred $M1$ and $E1$ strength function models result in a total radiation width definitely below the experimental value. This discrepancy, which to a lesser extent also shows up in the calculated quantities discussed below, may eventually be related to uncertainties of the average s-wave spacing $\langle D_0 \rangle$. Values of 44±4 eV, 65 eV, and 90±20 eV are reported in Refs. 46, 47, and 50, respectively, for this quantity; our calculations are based on the value of Ref. 47.

B. Capture cross sections

Figures 6–9 display calculated and experimental capture cross sections. The calculations were performed for both level density models and for the three different prescriptions for the $E1$ strength functions specified in Eqs. (2.1), (2.2), and (2.4); a standard Lorentzian was assumed as basis for $f_{M1}(\varepsilon_\gamma)$ and $f_{E2}(\varepsilon_\gamma)$. The figures do not contain all existing experimental data. We preferred those available in numerical form from the Nuclear Energy Agency (NEA) Data Bank[51] in the exchange format for experimental nuclear reaction data (EXFOR) format and used the graphical compilation by McLane *et al.*[52] to check that the data are representative.

In the range of incident energies considered here the different models for the $E1$ strength function mainly influence the magnitude but hardly the shape of the capture cross sections. In general, the shape of the experimental capture cross sections is well reproduced by the calculations. An exception is offered by the data of Bhohovko *et al.*[57] for ^{143}Nd which decrease faster with energy than our results. In the case of ^{197}Au(n,γ) for incident energies exceeding 1 MeV when the competing (n,n') reaction populates the continuum of ^{197}Au, the shape of the computed capture cross section depends on the level density model.

As far as the magnitude of the calculated capture cross section is concerned, one can observe a similar dependence on the gamma-ray strength functions and on the level densities as in the case of the total average s-wave radiation width. A standard Lorentzian with parameters derived from photoabsorption data for $E1$ radiation overpredicts the experimental capture cross sections. The best fits are obtained with a standard Lorentzian for $M1$ and a generalized one according to Eq. (2.4) for $E1$ radiation. However, in the case of ^{197}Au(n,γ), Eq. (2.2), i.e., the dotted curve in Figs. 6(a) and (b), also cannot be excluded.

The weak dependence of the shape of the capture cross section on the low-energy behavior of the gamma-ray strength functions provides the basis for the normalization procedures mentioned in the Introduction. As a drastic illustration we show in Fig. 10 again the capture cross section for ^{105}Pd calculated with the same three strength function models as before and the BSFG model for the level density. This time, however, we normalized the peak cross section for each of the three models of $f_{E1}(\varepsilon_\gamma)$ in such a way that a total s-wave radiation width of 145 meV results (see Table III); the normalization constants corresponding to Eqs. (2.1), (2.2), and (2.4) are 0.31, 2.40, and 0.83, respectively. As the level density parameters reproduce the average spacing $\langle D_0 \rangle$ the three different sets of strength functions correspond to the same value of $\langle \Gamma_{\gamma 0} \rangle / \langle D_0 \rangle$. Figure 10 shows that the resulting capture cross sections hardly differ from each other and reproduce the experimental data reasonably well. However, the three models for $f_{E1}(\varepsilon_\gamma)$ differ in shape and those given by Eqs. (2.1) and (2.2) correspond to a peak cross section not supported by photoabsorption data. This example shows that such a normalization is useful for applications if reliable information on $\langle \Gamma_{\gamma 0} \rangle$ and

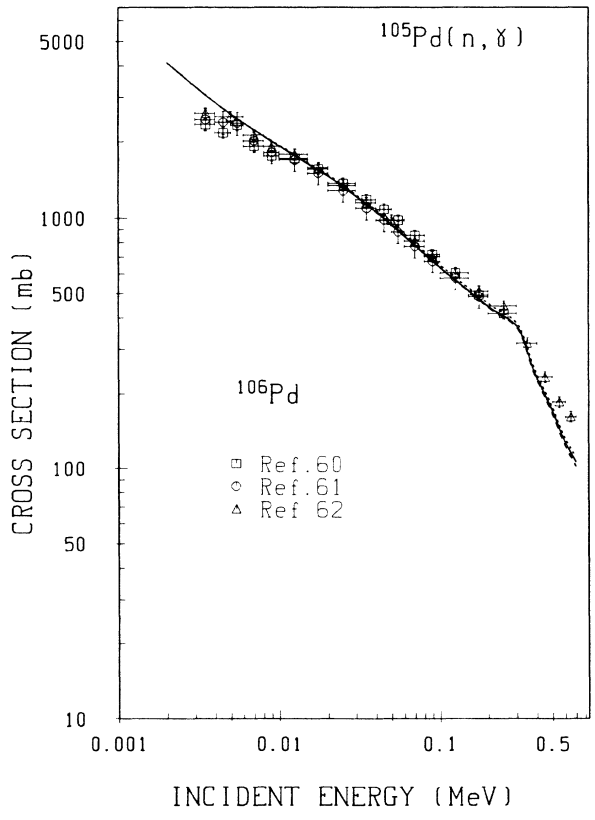

FIG. 10. The effect of strength function normalizations on the neutron capture cross section of ^{105}Pd. The $M1$ and $E2$ strength functions are derived from a standard Lorentzian. The BSFG model was chosen for the level density. The dashed, dotted, and full curves are obtained with $E1$ strength functions according to Eqs. (2.1), (2.2), and (2.4), respectively. In contrast to Fig. 8, however, in each case the peak cross section is chosen so as to reproduce the experimental value 145 meV of the total average radiation width. The experimental data are those of Fig. 8.

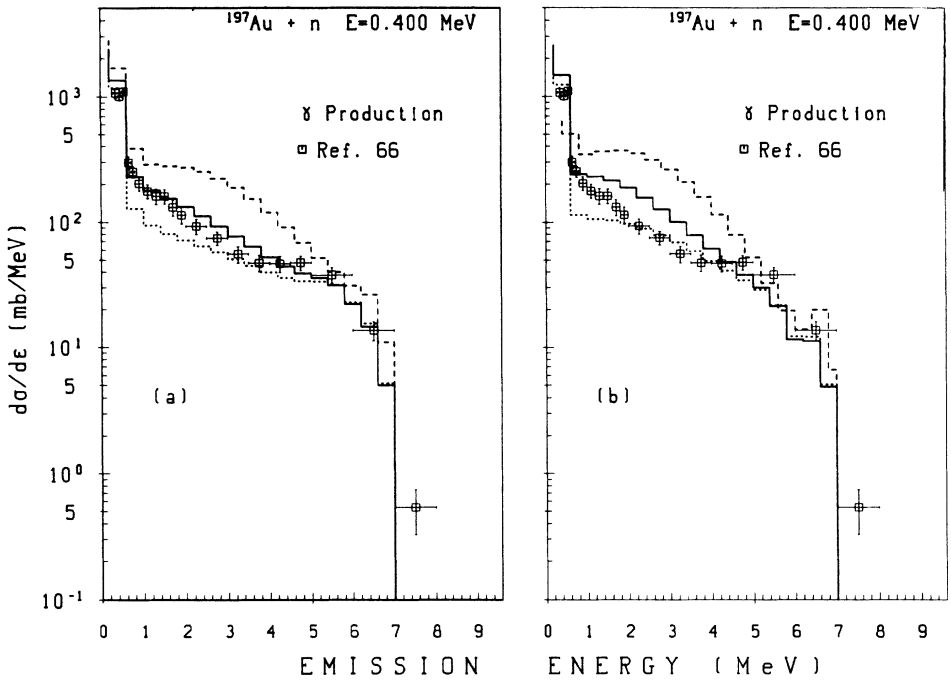

FIG. 11. The gamma-ray spectrum resulting from the reaction ^{197}Au$(n,x\gamma)$ at an incident energy of 0.4 MeV. The calculations are performed with level densities according to (a) the KRK model and (b) the BSFG model. The strength functions of $M1$ and $E2$ radiation were derived from giant resonances of Lorentzian shape. The dashed, dotted, and full histograms correspond to the three different prescriptions for the $E1$ strength function represented by Eqs. (2.1), (2.2), and (2.4), respectively. The experimental data (Ref. 66) are given for the incident energy interval 0.2–0.6 MeV and correspond to an emission angle of 125°. For the comparison with the calculations, isotropic emission was assumed.

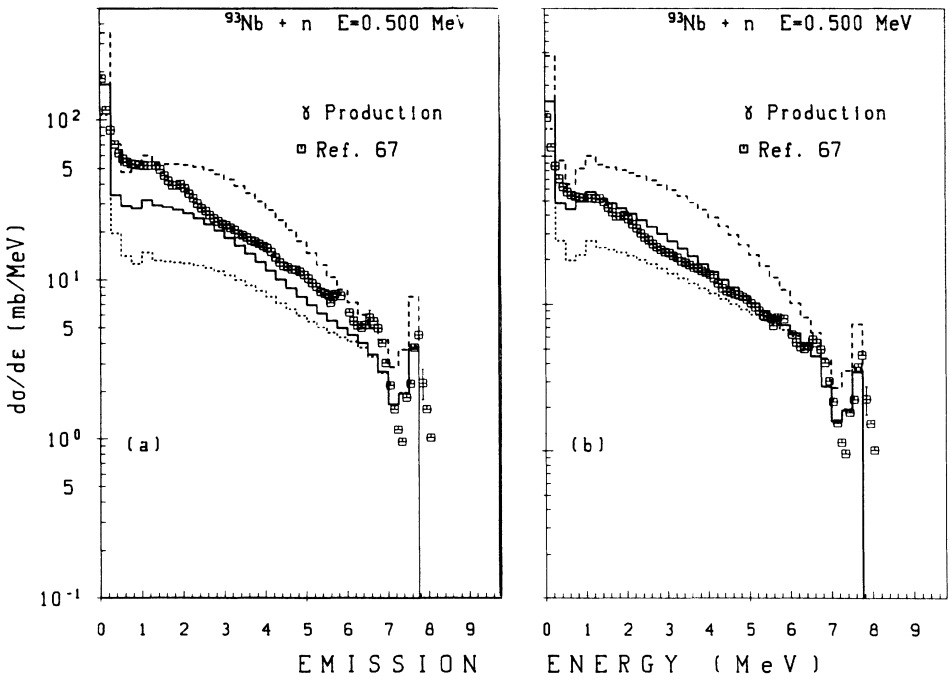

FIG. 12. The gamma-ray spectrum resulting from the reaction ^{93}Nb$(n,x\gamma)$ at an incident energy of 0.5 MeV. (a) and (b) and the different histograms have the same meaning as in Fig. 11. The experimental data were taken from Voignier *et al.* (Refs. 63 and 67); below an emission energy of 1.5 MeV the authors extrapolated the measurements by means of model calculations. For the comparison to our calculations we assumed isotropic emission.

$\langle D_0 \rangle$ is available. On the other hand, a good reproduction of experimental capture cross sections by this method alone does not guarantee that the underlying strength functions are correct in the sense that they reproduce independent experimental information.

C. Gamma-ray spectra

In the energy range considered, the average total radiation width and the capture cross sections essentially provide similar integral information on the gamma-ray strength. Further details can be learned from the analysis of gamma-ray spectra since their magnitude and shape depend on the strength functions.

Unfortunately we found experimental fast neutron capture gamma-ray spectra for only two of the nuclei considered. For ^{197}Au(n,γ) we used data measured by Morgan and Newman[66] and for ^{93}Nb(n,γ) those reported by Voignier *et al.*[63,67] Both data sets are confirmed by the results of other authors, too. We considered in each case only the spectra at the lowest incident neutron energy. Figures 11 and 12 display a comparison of these experimental data to model calculations performed for both level density models and the three different prescriptions for $f_{E1}(\varepsilon_\gamma)$ specified in Eqs. (2.1), (2.2), and (2.4). For $M1$ and $E2$ radiation a standard Lorentzian was again adopted. The reproduction of the high-energy end of the spectra is essentially improved by including the pigmy resonance to the $E1$ strength functions as given by Eqs. (2.2) and (2.4). For ^{197}Au(n,γ) the pigmy resonance was the object of many investigations; recent examples are those by Igashira *et al.*[8] and by Yamamuro *et al.*[68] In an analysis of the thermal capture spectrum of ^{93}Nb(n,γ) Gardner *et al.*[31] used, among other means to reproduce the high-energy end, a pigmy resonance also.

In this paper our main interest is not in the high-energy end nor in the pigmy resonance but in the low-energy portion of the gamma-ray spectra. Figures 11 and 12 clearly show that for emission energies between 1 and about 4 MeV the shape of spectrum depends on the model for $f_{E1}(\varepsilon_\gamma)$. Of particular interset is the difference between the full and the dotted histogram i.e., the calculation with a Lorentzian with an energy depending spreading width [Eq. (2.2)] and one which, in addition, contains the term responsible for the nonzero $\varepsilon_\gamma \to 0$ limit [Eq. (2.4)], because they represent models for the $E1$ strength function which cannot be distinguished by primary cap-

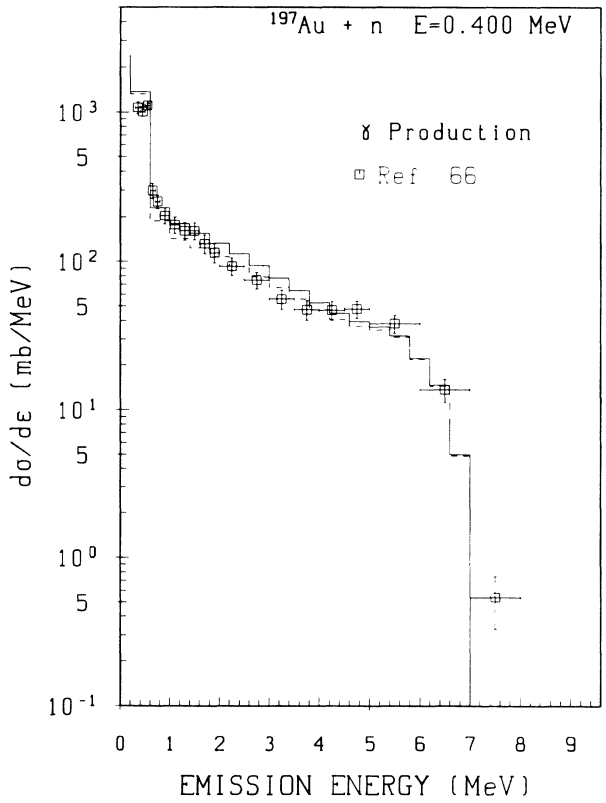

FIG. 13. The gamma-ray spectrum resulting from the reaction ^{197}Au$(n,x\gamma)$ at an incident energy of 0.4 MeV. The calculations are performed with the KRK model. The full histogram corresponds to a standard Lorentzian for $f_{M1}(\varepsilon_\gamma)$ and a generalized Lorentzian according to Eq. (2.4) for $f_{E1}(\varepsilon_\gamma)$. For the dashed histogram the adjusted single-particle model is assumed for $f_{M1}(\varepsilon_\gamma)$ and a Lorentzian with energy dependent spreading width according to Eq. (2.2) for $f_{E1}(\varepsilon_\gamma)$. Everything else is as in Fig. 11.

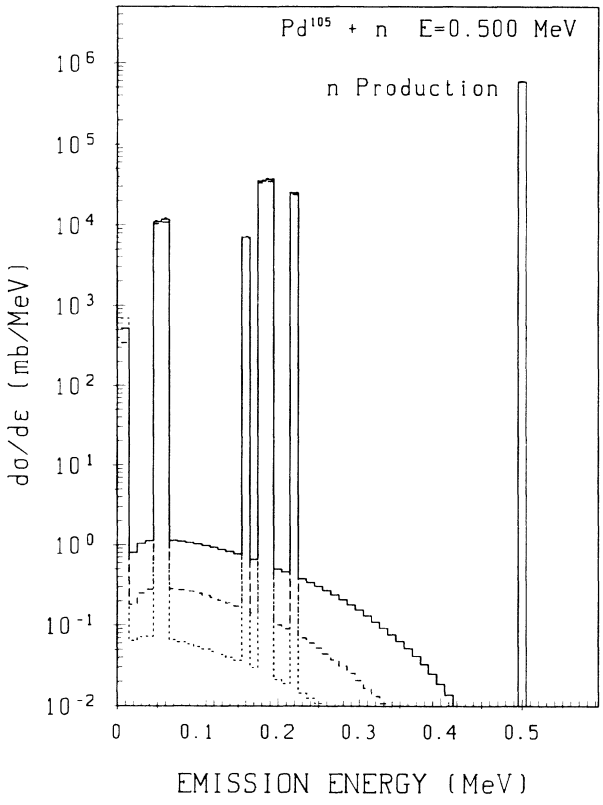

FIG. 14. The spectrum of neutrons resulting from the reaction ^{105}Pd$(n,\gamma n)$ at an incident energy of 0.5 MeV. The KRK model is used for the level density. The $M1$ and $E2$ strength functions are derived from standard Lorentzians. The dashed, dotted, and full curves correspond to $E1$ strength functions derived from Eqs. (2.1), (2.2), and (2.4), respectively.

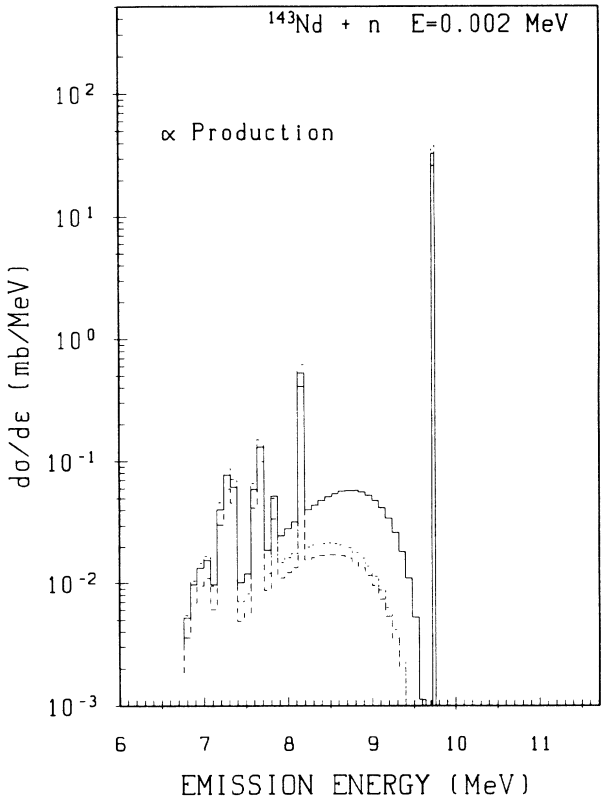

FIG. 15. The spectrum of alpha particles resulting from the reaction ^{143}Nd$(n,\gamma\alpha)$ at an incident energy of 2 keV. The same assumptions as in Fig. 14 are made regarding the level density model and the gamma-ray strength functions.

ture gamma rays. The experimental data for the reaction ^{197}Au(n,γ) at $E_n=0.4$ MeV (see Fig. 11) and also at 0.6 and 1.25 MeV (not shown) clearly favor the $E1$ strength function based on the generalized Lorentzian given in Eq. (2.4), while the capture cross section is also compatible with Eq. (2.2) (see Fig. 6). This conclusion is also valid for the reaction ^{93}Nb(n,γ) (see Fig. 12). Experimental gamma-ray spectra for ^{105}Pd(n,γ) also covering the low-energy end would be very helpful to gain further evidence for this $E1$ strength function model due to the accurate and extensive primary capture gamma-ray data available for this nucleus.

The analysis of gamma-ray spectra represents further support for an $E1$ strength function with a nonzero $\varepsilon_\gamma \rightarrow 0$ limit depending on the nuclear temperature. Of course, here one could also expect that $f_{E1}(\varepsilon_\gamma)$ based on Eq. (2.2) and the adjusted single-particle model for $f_{M1}(\varepsilon_\gamma)$ produce similar spectra. That this is indeed the case is shown in Fig. 13 where we compare for ^{197}Au(n,γ) at $E=0.4$ MeV these two possibilities with the KRK model for the level density. However, we refer again to the arguments against the adjusted single-particle model for the $M1$ strength presented in Sec. II.

D. Spectra of particles following gamma-ray emission

For completeness we mention that for small incident energies the spectra of particles emitted after gamma rays very sensitively depend on the presence of a nonzero $\varepsilon_\gamma \rightarrow 0$ limit of the electric (or magnetic) dipole strength. As illustration we show in Figs. 14 and 15 the neutron and alpha spectra from the reactions ^{105}Pd$(n,\gamma n)$ and ^{143}Nd$(n,\gamma\alpha)$ calculated at incident energies of 0.5 MeV and 2 keV, respectively. Alpha transmission coefficients were generated by means of an optical potential given by McFadden and Satchler.[69] The calculations employed the KRK model for the level density and were performed for the three models for the $E1$ strength functions. A strong enhancement of the continuous portion of the spectra as a consequence of the nonzero $\varepsilon_\gamma \rightarrow 0$ limit can be observed. These calculations refer to average cross sections and therefore cannot directly be compared to the results of Aldea *et al.*[21] who performed measurements of the alpha spectra resulting from the reaction ^{144}Nd$(n,\gamma\alpha)$ with thermal neutrons.

V. CONCLUSION

The results of the described model calculations critically depend on the strength function behavior of $E1$ and $M1$ radiation at low energies ε_γ where no direct experimental information on these quantities is available. By studying the impact of strength functions which simultaneously reproduce photoabsorption and/or average resonance data, but differ for low energies, model calculations can be used to test their low-energy behavior.

We pursued this program by analyzing data for four spherical nuclei with masses between 93 and 197. By combining all results we find strong support for a representation[14] of the $E1$ strength function that is based on a Lorentzian with energy dependent spreading width and exhibiting a nonzero $\varepsilon_\gamma \rightarrow 0$ limit depending on the nuclear temperature. These features of $f_{E1}(\varepsilon_\gamma)$ which imply a partial breakdown of Brink's hypothesis, are described in theoretical papers by Kadmenskij[19] and Sirotkin.[20] The effect of a nonzero $\varepsilon_\gamma \rightarrow 0$ limit could also be produced by an energy independent $M1$ strength adjusted to average resonance data. However, the strength of low-energy gamma-ray transitions does not confirm the adjusted single-particle model for $M1$ radiation.

These investigations of gamma-ray strength functions by means of model calculations should be extended to other mass regions and, in particular, to deformed nuclei. If the generalized Lorentzian with the nonzero $\varepsilon_\gamma \rightarrow 0$ proves universally valid it would be of considerable importance for all nuclear reaction model calculations.

ACKNOWLEDGMENTS

One of the authors (J.K.) appreciates a long collaboration on this subject with R. E. Chrien. All calculations were performed on an IBM 3090-400E VF computer installed at the University of Vienna in the frame of the European Academic Supercomputing Initiative (EASI) of the IBM Corporation. We acknowledge the help of the staff of the Vienna University Computer Center.

[1]M. Blatt and V. F. Weisskopf, *Theoretical Nucelar Physics* (Wiley, New York, 1952).
[2]Carol M. McCullagh, M. L. Stelts, and R. E. Chrien, Phys. Rev. C **23**, 1394 (1981).
[3]S. Raman, Inst. Phys. Conf. Ser. **62**, 357 (1981).
[4]D. M. Brink, Ph. D. thesis, Oxford University, 1955.
[5]P. Axel, Phys. Rev. **126**, 671 (1962).
[6]G. A. Bartholomew, E. D. Earle, A. J. Fergusson, J. W. Knowles, and A. M. Lone, Adv. Nucl. Phys. **7**, 229 (1973).
[7]G. Reffo, F. Fabbri, K. Wisshak, and F. Käppler, Nucl. Sci. Eng. **80**, 630 (1982).
[8]M. Igashira *et al.*, Nucl. Phys. **A457**, 301 (1986).
[9]S. Joly, Nucl. Sci. Eng. **94**, 94 (1986).
[10]R. L. Macklin and P. G. Young, Nucl. Sci. Eng. **95**, 189 (1987).
[11]J. Kopecky, Netherlands Energy Research Foundation Report No. ECN-99, 1981.
[12]W. V. Prestwitch, M. A. Islam, and T. J. Kennett, Z. Phys. A **315**, 103 (1984).
[13]J. Kopecky, *Proceedings of the International Conference on Nuclear Data for Basic and Applied Science, Santa Fe, 1985* (Gordon and Breach, New York, 1986), p. 967.
[14]J. Kopecky and R. E. Chrien, Nucl. Phys. **A468**, 285 (1987).
[15]S. Joly, D. M. Drake, and L. Nilsson, Phys. Rev. C **20**, 2072 (1979).
[16]D. G. Gardner and F. S. Dietrich, *Proceedings of the International Conference on Nuclear Cross Sections for Technology, Knoxville, 1979,* Natl. Bur. Stand. (U.S.) Spec. Publ. No. 594 (U.S. GPO, Washington, D.C., 1980), p. 770.
[17]B. J. Allen, I. Bergqvist, R. E. Chrien, D. Gardner, and W. Poenitz, *Neutron Radiative Capture* (Pergamon, New York, 1982), p. 62.
[19]D. F. Zaretskij and V. K. Sirotkin, Yad. Fiz. **27**, 1534 (1978) [Sov. J. Nucl. Phys. **27**, 808 (1978)].
[19]S. G. Kadmenskij, V. P. Markushev, and V. I. Furmann, Yad. Fiz. **37**, 277 (1983) [Sov. J. Nucl. Phys. **37**, 165 (1983)].
[20]V. K. Sirotkin, Yad. Fiz. **43**, 570 (1986) [Sov. J. Nucl. Phys. **43**, 362 (1986)].
[21]L. Aldea *et al.*, Z. Phys. A **283**, 391 (1977).
[22]G. A. Leander, Phys. Rev. C **38**, 728 (1988).
[23]C. B. Dover, R. H. Lemmer, and F. J. W. Hahne, Ann. Phys. (N.Y.) **70**, 458 (1972).
[24]C. A. Gosset *et al.*, Inst. Phys. Conf. Ser. **88**, 267 (1988).
[25]R. E. Chrien, Procedings of the Vth International School on Neutron Physics, Alushta, Dubna, 1987 (unpublished).
[26]J. Kopecky and R. E. Chrien, Inst. Phys. Conf. Ser. **88**, 702 (1988).
[27]A. G. Bohr and B. R. Mottelson, *Nuclear Structure* (Benjamin, London, 1975), Vol. II, p. 636.
[28]J. Kopecky, Inst. Phys. Conf. Ser. **62**, 423 (1982).
[29]J. Speth and A. van der Woude, Rep. Prog. Phys. **44**, 719 (1981).
[30]U. Mayerhofer *et al.*, Nucl. Phys. **A492**, 1 (1989).
[31]M. A. Gardner and D. G. Gardner, *Proceedings of the International Conference on Neutron Physics and Nuclear Data for Reactors and Other Applied Purposes, AERE Harwell, United Kingdom, 1978* (Organization for Economic Co-Operation and Development, Nuclear Energy Agency, Paris, 1978), p. 1121.
[32]S. S. Dietrich and B. L. Berman, At. Nucl. Data Tables **38**, 199 (1989).
[33]P. M. Endt, At. Nucl. Data Tables **26**, 47 (1981).
[34]J. Kopecky (unpublished).
[35]M. Schumacher, U. Zurmühl, F. Smend, and R. Nolte, Nucl. Phys. **A438**, 493 (1985).
[36]M. Uhl (unpublished).
[37]P. A. Moldauer, Nucl. Phys. **A344**, 185 (1980).
[38]B. Strohmaier and M. Uhl, *STAPRE—A Statistical Model Code with Consideration of Preequilibrium Decay,* Proceedings of the Course on Nuclear Theory for Applications, Trieste, Italy, 1978 (International Atomic Energy Agency, Vienna, 1980), p. 313.
[39]D. Wilmore and P. E. Hodgson, Nucl. Phys. **55**, 673 (1964).
[40]H. A. J. Van der Kamp and H. Gruppelaar, Netherlands Energy Research Foundation Report No. ECN-108, 1981.
[41]J. P. Delaroche, Ch. Lagrange, and J. Salvy, *Proceedings of the IAEA Consultants' Meeting on the Use of Nuclear Theory in Neutron Nuclear Data Evaluation, Trieste, 1975* (International Atomic Energy, Vienna, 1976), Vol. I, p. 251.
[42]R. L. Auble, Nucl. Data Sheets, **40**, 301 (1983); B. Harmatz, *ibid.* **34**, 101 (1983); J. K. Tuli, *ibid.* **56**, 607 (1989); L. K. Peker, *ibid.* **48**, 753 (1986); D. De Frenne, E. Jacobs, M. Verboven, and G. De Smet, *ibid.* **53**, 73 (1988); D. De Frenne, E. Jacobs, M. Verboven, and P. De Gelder, *ibid.* **47**, 261 (1986); H. W. Müller, *ibid.* **44**, 277 (1985); H. Sievers, *ibid.* **54**, 1 (1988).
[43]W. Dilg, W. Schantl, H. Vonach, and M. Uhl, Nucl. Phys. **A217**, 269 (1973).
[44]S. K. Kataria, V. S. Rhamaurthy, and S. S. Kapoor, Phys. Rev. C **18**, 549 (1978).
[45]S. F. Mughabgab, *Neutron Cross Sections* (Academic, New York, 1984), Vol. I, Part B.
[46]S. F. Mughabgab, M. Divadeenam, and N. E. Holden, *Neutron Cross Sections* (Academic, New York, 1981), Vol. 1, Part A.
[47]P. Vertes and Y. V. Grigoryew, *Proceedings of the International Conference on Nuclear Data for Science and Technology, Mito, Japan, 1988* (Saikon, Japan, 1988), p. 623.
[48]A. Gilbert and A. G. W. Cameron, Can. J. Phys. **43**, 1446 (1965).
[49]J. Winter *et al.*, *Proceedings of the International Conference on Neutron Physics and Nuclear Data for Reactors and Other Applied Purposes, AERE Harwell, United Kingdom, 1978* (Organization for Economic Co-Operation and Development, Nuclear Energy Agency, Paris, 1978), p. 696.
[50]G. Delfini and H. Gruppelaar, Netherlands Energy Research Foundation Report No. ECN-82, 1980.
[51]Organization for Economic Co-Operation and Development, Nuclear Energy Agency, NEA Data Bank, 91191 Gif-sur-Yvette CEDEX, France.
[52]V. McLane, C. L. Dunford, and Ph. F. Rose, *Neutron Cross Sections* (Academic, New York, 1988), Vol. 2.
[53]P. Andersson *et al.*, Nucl. Phys. **A443**, 404 (1985).
[54]A. N. Davletshin *et al.*, At. Energ. **58**, 731 (1983).
[55]H. A. Husain and S. E. Hunt, Int. J. Appl. Radiat. Isot. **34**, 731 (1983).
[56]Chen Jing, Zhu Sheng-Yun, Luo De-Xing, and Jiang Song-Chen, Chin. J. Nucl. Phys. **3**, 52 (1981).
[57]M. V. Bokovko *et al.*, Vopr. At. Nauk. I Tekh., Ser. Jad. Konst. **3**, 12 (1985).
[58]A. R. del Musgrove, B. J. Allen, J. W. Boldemann, and R. L. Macklin, *Nonstatistical Effects in Radiative Capture Cross Sections of the Neodynium Isotopes* (Australian Atomic Energy Commission, New South Wales, 1977; Nucl. Sci. Eng. **82**, 230 (1982).
[59]Y. Nakajima, A. Asami, Y. Kawarasaki, and Y. Furuta, *Proceedings of the International Conference on Neutron Physics and Nuclear Data for Reactors and Other Applied Purposes,*

AERE Harwell, United Kingdom, 1978 (Organization for Economic Co-Operation and Development, Nuclear Energy Agency, Paris, 1978), p. 438.

[60]E. Cornelis *et al.*, *Proceedings of the International Conference on Nuclear Data for Science and Technology, Antwerp, 1982* (Reidel, Dordrecht, 1982), p. 222.

[61]A. R. del Musgrove, B. J. Allen, J. W. Boldemann, and R. L. Macklin, *Proceedings of the International Conference on Neutron Physics and Nuclear Data for Reactors and Other Applied Purposes, AERE Harwell, United Kingdom, 1978* (Organization for Economic Co-Operation and Development, Nuclear Energy Agency, Paris, 1978), p. 449.

[62]R. L. Macklin, J. Halperin, and R. R. Winters, Nucl. Sci. Eng. **71**, 182 (1979); **78**, 110 (1981).

[63]J. Voignier, S. Joly, and G. Grenier, Nucl. Sci. Eng. **93**, 43 (1986).

[64]R. L. Macklin, Nucl. Sci. Eng. **59**, 12 (1976).

[65]W. P. Poenitz, Argonne National Laboratory Report No. ANL/NDM-8, 1974.

[66]G. L. Morgan and E. Newman, Oak Ridge National Laboratory Report No. ORNL-TM-4973, 1975.

[67]J. Voignier, S. Joly, and G. Grenier, Nucl. Sci. Eng. **96**, 343 (1987).

[68]N. Yamamuro, K. Udagawa, and T. Natsume, Nucl. Sci. Eng. **96**, 210 (1987).

[69]L. McFadden and G. R. Satchler, Nucl. Phys. **84**, 177 (1966).